Article

Not peer-reviewed version

Barrier-Free Carrier Injection in 2D $WSe_2/MoSe_2$ Heterostructures via Fermi-Level Depinning

Tian-Jun Dai *, Xiang Xiao , Zhong-Yuan Fan , Zi-Yan Zhang , Yi Zhou , Yong-Chi Xu , Jian Sun , Xue-Fei Liu *

Posted Date: 9 April 2025

doi: 10.20944/preprints202504.0739.v1

Keywords: WSe2/MoSe2 heterostructures; Fermi level pinning; Schottky barrier height; buffer layer; carrier injection efficiency

 doi:10.20944/preprints202504.0739.v1

Article

Barrier-Free Carrier Injection in 2D $WSe_2/MoSe_2$ Heterostructures via Fermi-Level Depinning

Tian-Jun Dai [1,*], Xiang Xiao [1], Zhong-Yuan Fan [1], Zi-Yan Zhang [1], Yi Zhou [1], Yong-Chi Xu [1], Jian Sun [1] and Xue-Fei Liu [2,3,*]

[1] School of Electronic Information Engineering, Guiyang University, Guiyang 550005, China
[2] School of physics and electronic science, Guizhou Normal University, Guiyang, 550025, China
[3] School of Integrated Circuit, Guizhou Normal University, Guiyang, 550025, China
* Correspondence: daitianjun7227@163.com (T.-J.D.); 201307129@gznu.edu.cn (X.-F.L.)

Abstract: Transition metal dichalcogenide (TMDC)-based two-dimensional (2D) type-II van der Waals heterostructures exhibit remarkable potential in next-generation optoelectronics, valleytronics, and spintronics. Nevertheless, the inevitable Fermi level pinning (FLP) effect at metal/TMDC interfaces intrinsically leads to elevated Schottky barrier heights (SBHs) and consequent contact resistance degradation. In this work, we present a first-principles investigation on the interfacial physics of metal-contacted $WSe_2/MoSe_2$ heterostructures with four representative electrodes (Ag, Al, Au, Pt). All the metal-$WSe_2/MoSe_2$ contacts induce significant metal-induced gap states (MIGSs), which are responsible for FLP inside the $WSe_2/MoSe_2$ band gaps. Ag-$MoSe_2$ contact has the minimum electron SBH of 0.31 eV, where the Pt-WSe_2 exhibits a minimum hole SBH of 0.43 eV. Upon inserting a 2D metal-doped metallic mWSe/mMoSe layer between $WSe_2/MoSe_2$ layer and metal electrodes, the MIGSs arising from the penetration of metal wave functions into the semiconductor layers can be effectively suppressed, leading to practically negligible SBHs both for electron and hole, and even a vanishing SBH is obtained, suggesting a high carrier injection efficiency. The achieved quasi-Ohmic contact characteristics provide a universal design paradigm for high-performance TMDC-based devices requiring ultralow contact resistance.

Keywords: $WSe_2/MoSe_2$ heterostructures; Fermi level pinning; Schottky barrier height; buffer layer; carrier injection efficiency

1. Introduction

Among various two-dimensional (2D) materials, transition metal dichalcogenides (TMDCs) are attracting tremendous interest due to their promising applications in electronics [1,2], valleytronics [3], optoelectronics [4,5]and spintronics [6]. Specifically, dangling bond free surfaces of 2D TMDCs enable the flexible construction of van der Waals (vdWs) heterostructures, providing opportunities for developing new devices with advanced functions. The observation of moiré superlattice exciton states in WSe_2/WS_2 vdWs heterostructures experimentally provides an attractive platform for controlling excited states of matter [7]. Tunneling field effect transistors based on 2D TMDCs heterostructures with subthreshold swing smaller than 60 mV dec^{-1} were demonstrated previously [8,9]. Intriguingly, selection of appropriate TMDCs layers allows type II heterostructures to be constructed, in which the ultrafast dynamics of charge transfer across the vdWs interface and the spatial segregation of photo-generated holes and electrons can be achieved. The electron transfer from WSe_2 to MoS_2 taken place within 470 fs with 99% charge transfer efficiency in MoS_2/WSe_2 p-n heterojunctions was reported [10]. Policht et al. observed an ultrafast interlayer electron transfer of up to 69 fs in WS_2/MoS_2 type II band alignment by using 2D electronic spectroscopy [11]. Similar sub-ps level charge transfer processes were also demonstrated in $MoS_2/MoTe_2$, $MoSe_2/MoS_2$ and WSe_2/WS_2 heterostructures [12,13]. However, the photoresponse times drop to the order of μs when made these heterojunctions into optoelectronic devices [14,15].

 doi:10.20944/preprints202504.0739.v1

Inevitably, 2D TMDCs-based devices have contact interfaces with metal electrodes, and the quality of the electrical contacts becomes particularly important on their performances. 2D semiconductors generally exhibit unfavorable band edges due to the strong excitonic effect and quantum confinement [16], thus, for most commercially available metals (with the work function ranging from 3.5 eV to 5.7 eV) [17] the formation of low resistance ohmic contacts to mask the intrinsic exceptional properties of 2D TMDCs is still challenging to obtain [18]. The Schottky barrier height (SBH) at the metal-2D TMDCs interfaces, not simply depending on the difference between the work function of the metal and the conduction band minimum (CBM)/valence band maximum (VBM) of the TMDCs due to the complex Fermi level pinning (FLP), is a measure of the barrier to charge injection. A large SBH leads to high contact resistance at the metal-TMDCs interfaces, reducing the carrier injection efficiency [19,20]. Therefore, it is highly desirable to decrease SBH (a low resistance ohmic contact with vanishing SBH) to gain a high performance of a device.

A Schottky pinning factor S is normally introduced to describe the strength of the FLP, which is defined as the change in SBH (Φ_{SBH}) with respect to the metal work function (W_F), i.e., $S=|d\Phi_{SBH}/dW_F|$ [17,21,22]. Not that S is the slope of Φ_{SBH} versus W_F, typical values reported are in the range of 0~1 [17,21–23], where a value close to 0 corresponds to a strong pinning interface, and a weakly interacting metal-TMDCs system is achieved for S close to 1, indicative of approaching the ideal Schottky-Mott limit. The FLP effects can be normally attributed to the interfacial effects [24], surface traps [25] and metal-induced gap states (MIGSs) [24,26,27]. Several works reported that the FLP can be weakened by inserting a buffer layer between the TMDCs and metal experimentally and theoretically, such as hexagonal boron nitride (h-BN) [28,29], molybdenum trioxide (MoOx, x<3) [30], ultrathin TiO_2 [31], graphene [32,33], ZnO [34], monolayer (ML) NbS_2 [25], VS_2 [26], and so on. These results show that the introduction of buffer layers is an effective strategy to break the direct metal-TMDCs interaction and destroy the interface states, improving the contact properties.

Beyond their established advantages in ultrafast optoelectronics and emerging quantum information applications [35–37], $WSe_2/MoSe_2$ heterostructures present unique opportunities for fundamental interface engineering studies. Through density functional theory (DFT) simulations of four conventional metals (Ag, Al, Au, Pt) interfaced with monolayer $WSe_2/MoSe_2$ heterostructures, we reveal universal Schottky-type contacts with characteristic Fermi-level pinning. No ohmic contact is observed, $MoSe_2$ forms an N-type Schottky contact with Ag and Al electrodes with electron SBH of 0.31 and 0.88 eV, and a P-type Schottky contact with Pt and Au electrodes with hole SBH of 0.42 and 0.76 eV, respectively. A similar trend is also observed in metal-WSe_2 contacts, where the Pt-WSe_2 exhibits a minimum hole SBH of 0.43 eV. Furthermore, we also demonstrated that inserting a 2D materials metallic layer (mMoSe/mWSe) between the metals and $WSe_2/MoSe_2$ layer indeed weakens the interaction at the contacting interfaces, which can effectively suppress the MIGSs, depinning the Fermi level, and thus reducing all the SBHs significantly.

2. Computational Methods

We use the Projector Augmented Wave (PAW) method and plane wave basis set implemented in the Vienna ab initio simulation package (VASP) code to optimize the geometries [23,24]. Using the Perdew Burke Ernzerhof (PBE) exchange correction function to modify the generalized gradient approximation (GGA) function [38]. To ensure accuracy, the plane-wave cutoff energy is set to 600 eV. The Brillouin zone are sampled with special k-points of 5×5×1 for optimizing supercell structures and 10×10×1 for densities of states (DOS) calculations. DOS calculations are implemented by using Gaussian drag method with a drag width of 0.02 eV [39,40]. The calculation is considered complete only when the energy difference between two consecutive steps is less than 10^{-6} eV and the force acting on each atom is less than 0.01 eV/Å.

To accurately model metal electrode interfaces, six atomic layers of (111)-oriented Ag, Al, Au, and Pt slabs were employed based on converged surface properties established in prior studies [41,42]. The in-plane lattice constants of WSe_2 and $MoSe_2$ are a_1=3.29 Å and a_2=3.32 Å showed excellent agreement with experimental measurements [43,44]. A supercell with a lattice mismatch of less than

 doi:10.20944/preprints202504.0739.v1

5% is needed to get stable structures of heterojunctions. Thus, the pristine metals/WSe_2/$MoSe_2$ supercells are constructed using a 2×2 expansion of Ag, Al, Au, and Pt (111) and a$\sqrt{3}\times\sqrt{3}$ expansion of monolayer (ML) WSe_2/$MoSe_2$, resulting in lattice mismatches ranging from 0.21% to 3.56% as displayed in Tables 1. A vacuum layer exceeding 15 Å thickness was implemented along the z-direction to eliminate spurious interactions between periodic images.

3. Results and Discussion

Figures 1(a) and (b) illustrate the architecture of top-contact configurations where monolayer WSe_2/$MoSe_2$ interfaces with six-layer (111)-oriented metal slabs (Al, Ag, Au, Pt). The most stable configuration of the ML WSe_2/$MoSe_2$ on Ag and Au comes from the structure that the Se atoms are located at the center of a hexagon formed by six adjacent metal surface atoms, directly below the surface hollow site, where the W/Mo atoms are located above the center of a triangle formed by three neighboring metal atoms, as shown in Figure 1(a). Figure 1(b) displays the most stable configuration of Al- and Pt-WSe_2/$MoSe_2$ interfaces in which the W/Mo atoms sit above the center of the hexagons and Se atoms are above the centers of the triangles formed by metal atoms, respectively. Since the obtained results do not change appreciably beyond six layers of metal atoms [45], we restrict the simulation to this thickness. The equilibrium interfacial distances dz, defined as the difference between Se atoms and metal atoms along the z-direction (perpendicular to the interface) at the contact interfaces, varying from 2.488 to 2.912 Å, decreasing in the order of Al>Au>Ag>Pt (see Table 1). The binding energy of per interfacial Se atom is defined as

$$E_b = (E_{WSe2/MoSe2} + E_{metal} - E_{metal\text{-}WSe2/MoSe2})/N_{Se} \quad (1)$$

Where E_{metal}, $E_{WSe2/MoSe2}$, and $E_{metal\text{-}WSe2/MoSe2}$ are the relaxed energies for metal surface, WSe_2/$MoSe_2$, and the combined system per supercell, respectively, and N_{Se} is the number of Se atoms at the interface of each supercell. E_b ranges from 0.182 eV (Al-WSe_2) to 0.342 eV (Pt-$MoSe_2$) as listed in Table 1, demonstrating the bonding strength trend. It can be found that Pt has a relatively strong adsorption (E_b =0.318/0.342 eV) and a small distance (dz=2.53/2.488 Å) with WSe_2/$MoSe_2$, showing a relatively strong bonding compared to those of other metals.

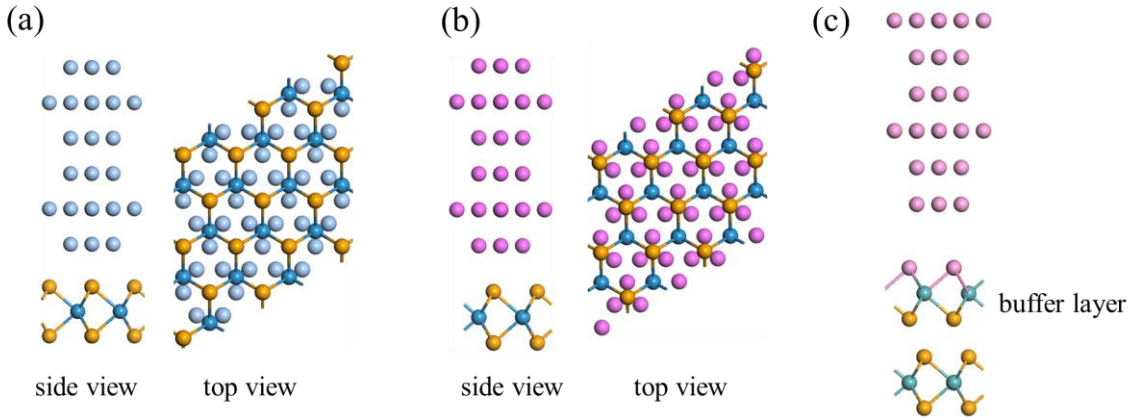

Figure 1. Interfacial geometries of contacts to ML WSe_2/$MoSe_2$. (a) Side and top views of Ag/Au (111)-WSe_2/$MoSe_2$ contacts. (b) Side and top views of WSe_2/$MoSe_2$ on Al/Pt (111) surfaces. (c) Side views of the metal-WSe_2/$MoSe_2$ contacts with a metal doped mMoSe/mWSe buffer layer inserted.

 doi:10.20944/preprints202504.0739.v1

Table 1. Calculated interfacial properties of WSe_2 and $MoSe_2$ on the metal electrodes. LM represents the lattice constant of the metals used in this article, with lattice mismatches in parenthesis below. d_Z is defined as the physical separation (the distance between the Se atoms and the topmost metal atomic layer in the z direction). E_b is the binding energy. W_M and W are the calculated work functions for clean metal and metal-WSe_2/$MoSe_2$ contacts, respectively. The SBHs extracted from band calculation without (with) inserting a buffer layer. (^{N}electron Schottky barrier, ^{P}hole Schottky barrier).

Metal	LM (Å)	WSe_2/$MoSe_2$				
		d_Z (Å)	E_b (eV)	W_M (eV)	W (eV)	SBH (eV)
Ag	5.778 (1.26/0.40%)	2.719/2.683	0.284/0.305	4.48	4.59/4.78	0.43^N/0.31^N (0.19^N/0.00^N)
Al	5.726 (0.36/0.49%)	2.912/2.784	0.182/0.205	4.11	4.37/4.62	1.1^N/0.88^N (0.04^N/0.02^N)
Au	5.767 (1.07/0.21%)	2.879/2.780	0.252/0.261	5.38	5.1/5.09	0.66^P/0.76^P (0.13^N/0.03^N)
Pt	5.549 (2.73/3.56%)	2.53/2.488	0.318/0.342	5.72	5.67/5.68	0.43^P/0.42^P (0.19^P/0.29^P)

Before performing the metal-TMDCs systems investigation, we obtain the band structures of pure ML $MoSe_2$ and WSe_2 layers (see Figure S1 in the supporting information). The results show that ML WSe_2/$MoSe_2$ is a semiconductor with a band gap of 1.63/1.51 eV, which is consistent with previously reported values [46,47]. Figure 2 shows the projected band structures of metal-ML WSe_2 combined systems where the band structures of metal-$MoSe_2$ systems are presented in Figure 3. Both majority bands of ML WSe_2 and $MoSe_2$ are still identifiable when contacted with Ag, Al, Au and Pt surfaces. Although the conduction bands of $MoSe_2$/WSe_2 is reserved well when contacted with Pt, as shown in Figure 2(d) and Figure 3(d), the valence bands exhibit a slight hybridization, which are related to the *d*-orbital radius and occupied level of metals [47]. Actually, the band hybridization degree in different metal-$MoSe_2$/WSe_2 interfaces can be explained by the d-band model [48]. Pt has partially occupied d-orbitals leads to stronger bond with $MoSe_2$/WSe_2 than that of Ag and Au (full d-shells), which can mix with the band-edge d-orbitals of W and Mo, resulting in a better electron injection efficiency. This result is in good agreement with the binding energy calculation. Accordingly, Al is not a good choice for metal-$MoSe_2$/WSe_2 contact owing to the absence of d-orbitals [41,46], and a high resistance contact of Al-TMDCs has been verified experimentally [49].

After formation of the contacts, the Schottky barriers appear in the vertical direction, and thus vertical Schottky barriers height can be precisely determined by $\Phi_n = E_{CBM}-E_F$ (electrons) and $\Phi_p = E_F-E_{VBM}$ (holes), where E_{CBM}, E_{VBM}, and E_F are the positions of the CBM, VBM, and Fermi level in the metal-$MoSe_2$/WSe_2 junctions, respectively. Φ_{SBH} is crucial for the optical and electrical properties of $MoSe_2$/WSe_2 device. As shown in Figures 2(a) and (b), in Ag- and Al-WSe_2 contacts, the Schottky barriers are N-type with electron SBHs of Φ_n= 0.43 and 1.1 eV, respectively. While in Au- and Pt-WSe_2 contacts (see Figures 2(c) and (d)), the vertical Schottky barriers exhibit P-type, giving hole SBHs of Φ_p =0.66 eV and 0.43 eV. The extracted SBHs values for various metal-WSe_2 combinations are listed in Table 1. Using a same approach, as displayed in Figure 3, SBHs for all of the metal-$MoSe_2$ systems are calculated, and the extracted electron/hole SBHs as given in Table 1. Similarly, the Schottky barriers are N-type with Φ_n=0.31 and 0.88 eV in Ag- and Al-$MoSe_2$, and are P-type with Φ_p = 0.76 eV and 0.42 eV in Au- and Pt-$MoSe_2$, respectively. In these contacts, the large Φ_n of Al-$MoSe_2$/WSe_2 indicating a high resistance in the contact interfaces, which is consistent with the previous analysis. Actually, the contact polarity of Au-WSe_2 has generally been reported to be ambipolar or P-type [50–

 doi:10.20944/preprints202504.0739.v1

52]. However, a predict N-type contact polarity could be realized with selenium vacancies [24]. A reported drop of P-type SBH from the transferred Au electrode (0.62 eV) to the evaporated Au electrode (0.19 eV) for WSe_2 ML devices [51], indicating that a SBH value can be tuned by different fabricated approaches. Moreover, For Pt-$MoSe_2$/WSe_2 contact systems, the vertical hole SBHs (0.42/0.43 eV) is comparable with the one (0.55/0.34 eV) reported by other works [46,47].

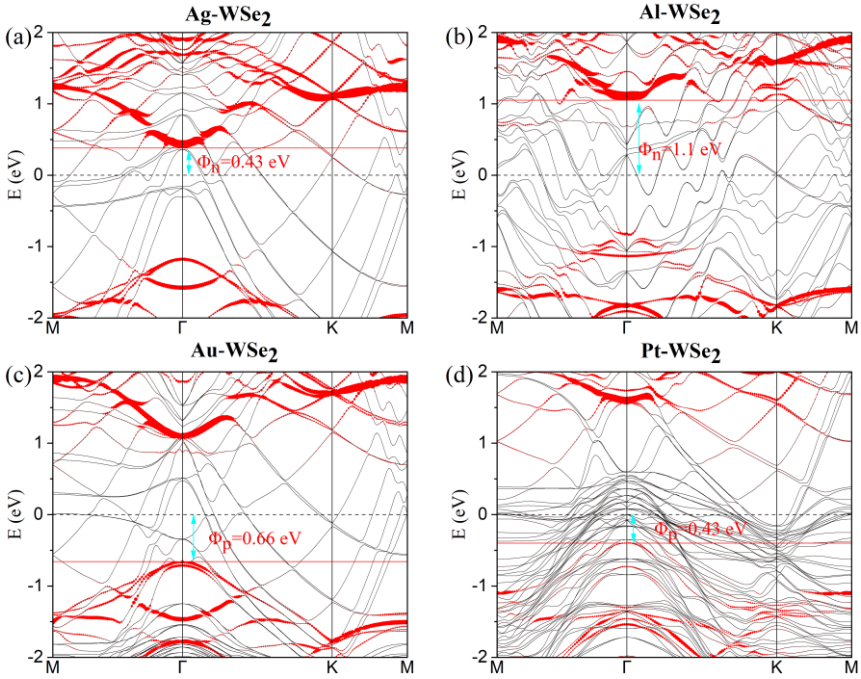

Figure 2. Band structures of ML WSe_2 contacting with several metal electrodes. The Fermi level is set to zero. (a)-(d) The bands dominated by metal atoms and ML WSe_2 are plotted by gray and red curves, respectively. The Schottky barrier is marked in green and red.

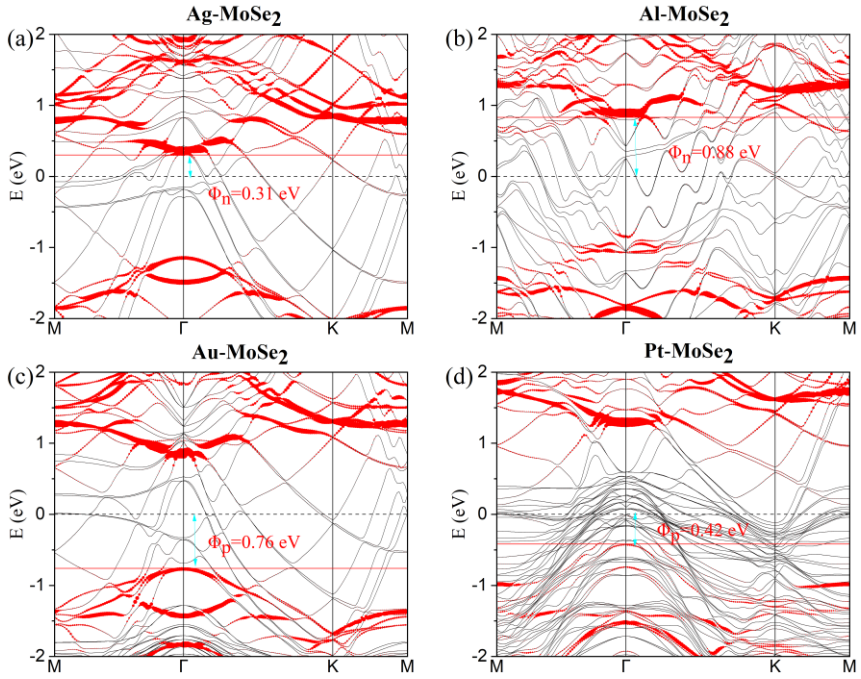

Figure 3. Band structures of ML $MoSe_2$ contacting with several metal electrodes. The Fermi level is set to zero. (a)-(d) The bands dominated by metal atoms and ML $MoSe_2$ are plotted by gray and red lines, respectively. The Schottky barrier is marked in green and red.

 doi:10.20944/preprints202504.0739.v1

Contact engineering is necessary to suppress the Φ_{SBH} of the metal-TMDCs systems with the goal to achieve a low resistance Ohmic contact for 2D devices. An ultrathin buffer layer is a technologically viable approach to reduce the Φ_{SBH}. It has been reported, for example, that a hBN buffer layer in Ni-MoS_2 contact can decrease the SBH from 0.158 to 0.031 eV [53]. Also, a graphene buffer layer is effective in reducing the SBH from 0.3 to 0.19 eV in Ag-MoS_2 configuration [54]. Moreover, thin oxides, such as Al_2O_3, have been used as buffer layer in Ti-MoS_2, reducing the SBH from 0.18 to 0.13 eV [55]. Here, we report the metal-doped $MoSe_2/WSe_2$ (mMoSe/mWSe) acts as a buffer that can be sandwiched between metal electrodes and 2D $MoSe_2/WSe_2$ semiconductors (as illustrated in Figure 1(c)). It is important to stress that the configuration of metal atoms replacing Se atoms required less formation energy and is more stable than that of replacing Mo/W atoms, and a mMoS layer has been realized via a three-step plasma-deposition-annealing yttrium-doping process experimentally [56]. The metal-doping means to covert semiconducting $MoSe_2/WSe_2$ into metallic mMoSe/mWSe is theoretically predicted. Au-doping is taken as an example (see Figure S2), the band structure of AuMoSe/AuWSe with the VBM as well as the CBM coinciding in the Brillouin zone, confirming the zero bandgap metallic characteristic. Figures 4(a)-(d) show the projected band structures of metal-mWSe-WSe_2 complexes. Obviously, after inserting an 2D mWSe layer into the contact interfaces, the barrier heights are reduced to 0.19, 0.04, 0.13 and 0.19 eV in the Ag-, Al-, Au- and Pt-mWSe-WSe_2 contacts, respectively. While for metal-mMoSe-$MoSe_2$ configurations, as shown in Figures 5(a)-(d), the corresponding vertical Schottky barriers are extracted to 0, 0.02, 0.03 and 0.29 eV, respectively. All the SBHs of electrons and holes are summarized in parentheses in Table 1. It is obvious that Φ_n is decreased significantly in the N-type contacts while Φ_P is relatively slight in the P-type contacts compared with those of without involving a buffer layer. Intriguingly, in contrast to the previous conclusion, the ultra-low Schottky barrier heights of Al-mMoSe/mWSe-$MoSe_2/WSe_2$ proves that Al becomes a good metal for low resistance contact after inserting the buffer layer. Furthermore, the transition from P-type contacts at Au-$MoSe_2/WSe_2$ interfaces to N-type contacts at Au-mMoSe/mWSe-$MoSe_2/WSe_2$ interfaces is observed. It is worth noting that a vanishing vertical N-type SBH in Ag-mMoSe-$MoSe_2$ combined system indicates a low resistance Ohmic or quasi-Ohmic contact (Figure 5(a)), implying a high carrier injection efficiency.

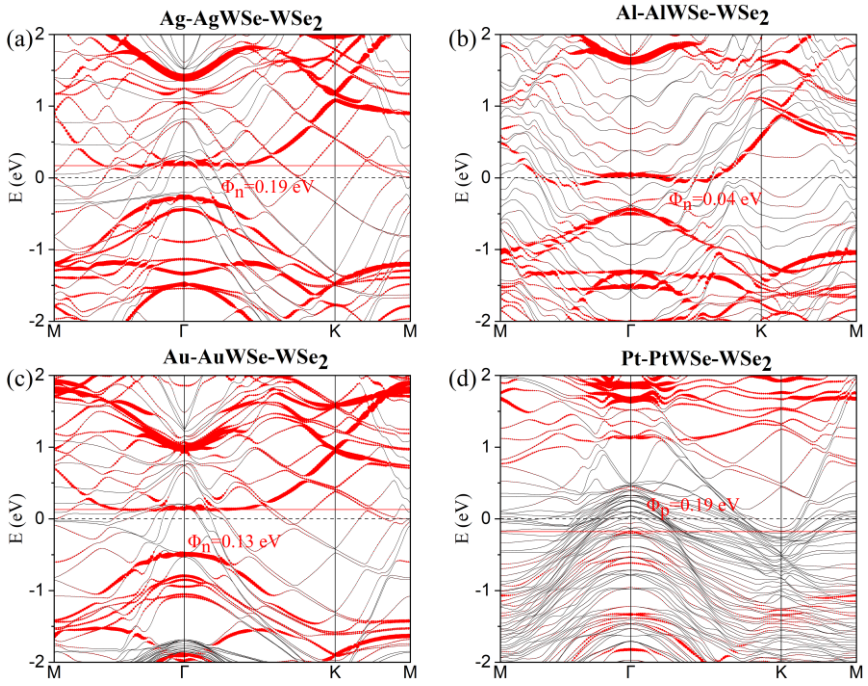

Figure 4. Projected band structures of several metals contact to ML WSe_2 with inserting mWSe buffer layers. The Fermi level is set to zero. Red line: energy bands dominated by WSe_2 layer, gray line: band structures of metals-mWSe systems.

 doi:10.20944/preprints202504.0739.v1

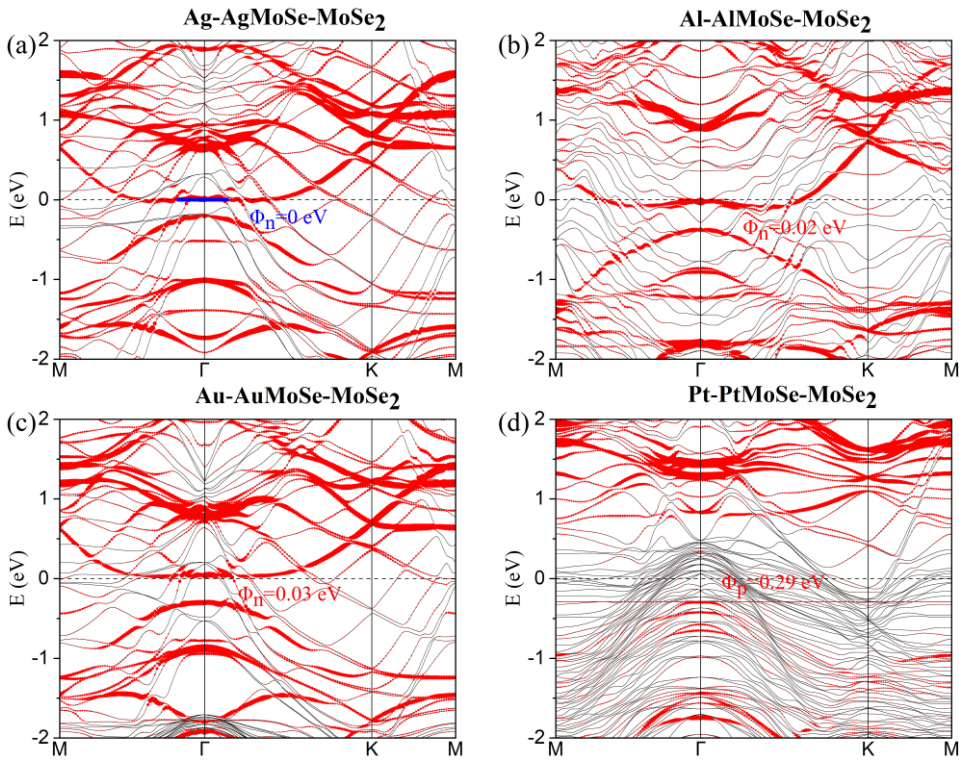

Figure 5. Projected band structures of several metals contact to ML $MoSe_2$ with inserting mMoSe buffer layers. The Fermi level is set to zero. Red line: energy bands dominated by $MoSe_2$ layer, gray line: band structures of metals-mMoSe systems.

Apparently, the extracted Φ_{SBH} for various configurations are different from the predicted values by straightforward band alignment estimation, which are ascribed to the Fermi level pinning effect at the interfaces. To further quantify the strength of pinning behavior in different contacts, we plot the work function dependent Φ_n between semiconductor $MoSe_2$/WSe_2 and various metals systems, as shown in Figure 6. It is found that the SBHs of metal-WSe_2 interfaces lie on a line of slope S=0.41, while those of metal-$MoSe_2$ contacts lie on a line of slope S=0.33 (see Figure 6(a)), deviating from ideal Schottky-mott limit, indicating a strong pinning effect. Nevertheless, it is worth noting that these values are much larger than that of conventional semiconductor combines (GaAs (0.07) and Si (0.27)) [57]. For comparison, as exhibited in Figure 6(b), we also extract the value of S factors with mMoSe/mWSe buffer layers inserted between the metals and $MoSe_2$/WSe_2. A large pinning factor close to 1 (0.79 for metal-mMoSe-$MoSe_2$ and 0.76 for metal-mWSe-WSe_2) indicates a depinning Fermi level effect, which can be attributed to the reduction of the MIGS density in the contact stacks due to a weakened interaction between the metal and $MoSe_2$/WSe_2 layer. It is reported that an increased metal-TMDCs distance also can effectively suppress the MIGSs, and thus depinning Fermi level, reducing the SBHs [23].

 doi:10.20944/preprints202504.0739.v1

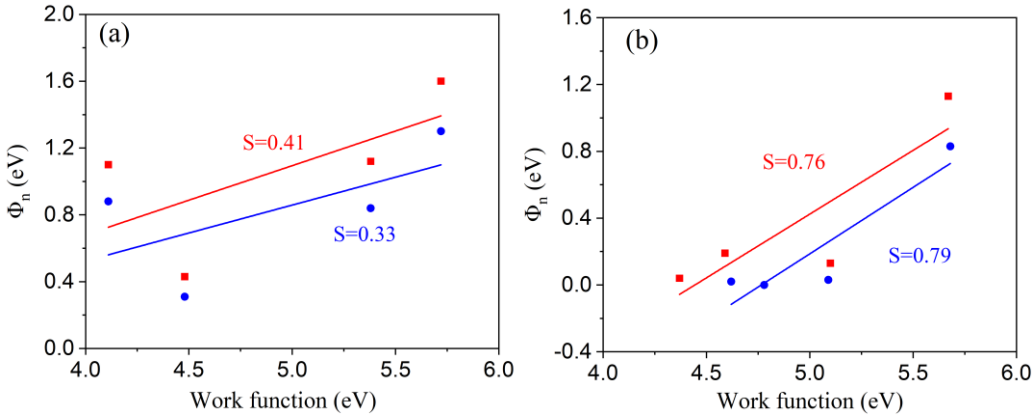

Figure 6. Variation of the Schottky barrier height of electrons (Φ_n) with change of the work function for metals systems (a) in metal-$MoSe_2$/WSe_2 stacks and (b) in metal-mMoSe/mWSe-$MoSe_2$/WSe_2 stacks. The red and blue solid lines are fitted curves for metal systems contact to WSe_2 and $MoSe_2$, respectively. Fermi level depinning is seen after inserting a mMoSe/mWSe buffer layer, with pinning factors increased significantly.

To deeply understand the effect of conventional metals or mMoSe/mWSe layers on the ML $MoSe_2$/WSe_2 semiconductor, we calculate the partial density of states (PDOS) of pristine $MoSe_2$/WSe_2 and the contact systems. As shown in Figures 7(a)-(d), after contacted with metal faces, significant MIGSs are induced in the original band gap of WSe_2 compared to that of the pristine WSe_2 without contact (see Figure S3), which is consistent with previous studies [17,46]. It is observed that much more overlap interface states distributed in the pristine band gap for Pt contact compared with those of in other contacts (Figure 7(d)), indicating a strong hybridization in Pt-WSe_2 combine, which is in agreement with the band structure hybridization degree. In contrast, as indicated in Figures 7(e)-(h), the corresponding metal-doped metallic mWSe in contact with ML WSe_2 has negligible metal-induced gap states, leading to almost no additional Fermi-level pinning, which can be attributed to the native ideal vdWs interfaces between the mWSe and WSe_2 layers. Moreover, similar contact nature trends are also obtained by comparing the PDOS in metal-$MoSe_2$ and mMoSe-$MoSe_2$ systems (see Figure S4 in the supporting information).

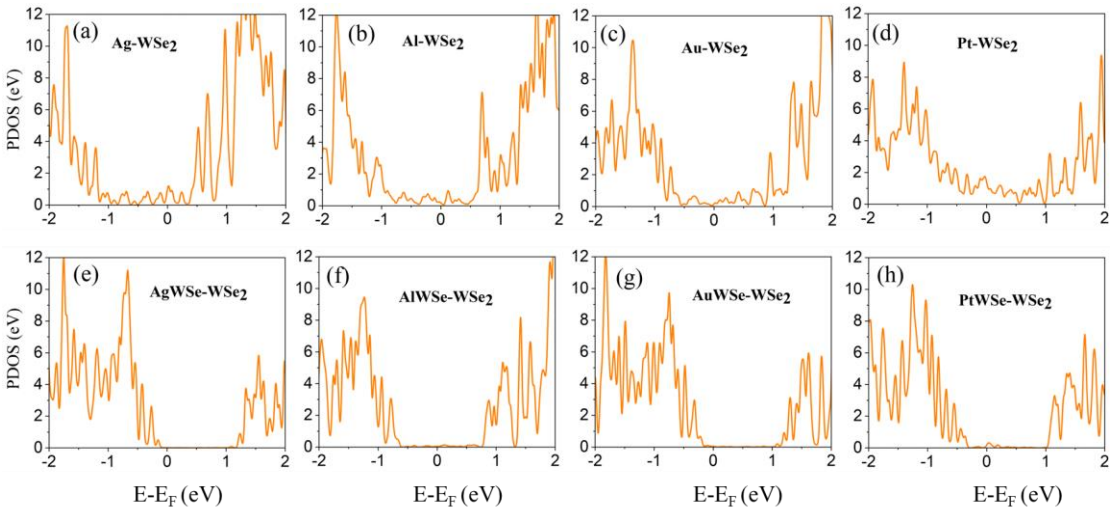

Figure 7. Partial density of states (PDOS) of WSe_2 after contact with (a)-(d) metals and (e)-(h) metallic mWSe surfaces for comparison. The Fermi level is at zero energy.

A prototype device (optoelectronic/electronic) based on $MoSe_2$-WSe_2 vdWs heterostructure consisting of a drain (D), a source (S) and a heterostructure channel is illustrated in Figure 8(a). dz measured from optimized geometries (Table 1) and a notably high ΔV, defined as the potential

 doi:10.20944/preprints202504.0739.v1

energy above E_F at the metal-WSe_2/$MoSe_2$ interfaces, is obtained (Figure S5), verifying the existence of tunneling barriers (TBs) [17,46]. In the light of TBs and Schottky barriers which are analyzed to evaluate the carrier injection efficiency of contacts, take N-type contact as an example, band diagrams for metal-WSe_2/$MoSe_2$ stacks and metal-interlayer-WSe_2/$MoSe_2$ stacks are shown in Figures 8(b) and (c), respectively. It is important to note that a narrow tunneling barrier and low Schottky barrier at metal-TMDCs interface can increase the carrier injection efficiency [17,18,46]. In the absence of buffer layer, a thin (even a vanishing) tunneling barrier is formed at the metal-WSe_2/$MoSe_2$ interface which is related to the band hybridization degree (Figure 8(b)). Although inserting a mMoSe/mWSe layer leads to a larger distance due to the nonbonding vdWs gap (~0.70 nm) between the mMoSe/mWSe and ML WSe_2/$MoSe_2$, resulting in a higher tunneling barrier, the weakened interaction at the interfaces can effectively suppress the formation of MIGSs (Figure 8(c)), thus reducing the SBHs.

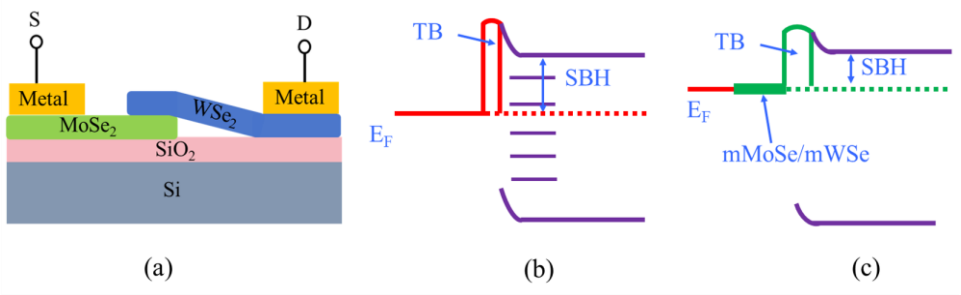

Figure 8. (a) Schematic diagram of a $MoSe_2$-WSe_2 heterostructure device. (b) Simplified band diagram for metal-$MoSe_2$/WSe_2 contacts, the SBH and TB depend on the type of metal, which are related to the band hybridization degree. (c) Sketch of the band diagram for metal-mMoSe/mWSe-$MoSe_2$/WSe_2 stacks. The barrier height is reduced by suppressing the penetration of MIGSs.

4. Conclusions

The strategic modulation of Schottky barrier heights (SBHs) for both carrier polarities constitutes a critical advancement in developing high-efficiency two-dimensional optoelectronic devices. In this work, we have systematically investigated the contact interfaces between WSe_2/$MoSe_2$ heterojunction and a set of metals with a wide range of work functions (Ag, Al, Au, and Pt). Our calculation results show that the directly contacting WSe_2/$MoSe_2$ with various elemental metals leads to partial FLP due to the large density of MIGSs, and the electron/hole SBHs can be modulated effectively by varying metals (with the relatively large values ranging from 0.31 eV for Ag-$MoSe_2$ contact to 1.11 eV for Al-WSe_2 contact). A larger value of S close to 1 can be obtained by inserting a metal-doped mWSe/mMoSe layer as a metallic buffer between the metals and the 2D WSe_2/$MoSe_2$ semiconductor, suggesting a depinning Fermi level effect. In the presence of a buffer layer, both the polarities of Au-$MoSe_2$ and Au-WSe_2 contacts change from P-type to N-type, and all the SBHs can be reduced to a small even negligible value due to the suppression of MIGSs, implying a low resistance Ohmic contact. Our studies provide a theoretical reference for designing of high-performance 2D TMDCs devices.

Supplementary Materials: The following supporting information can be downloaded at the website of this paper posted on Preprints.org.

Acknowledgments: This work was supported by the National Natural Science Foundation of China (No. 62264001), the Provincial Basic Research Program project of Guizhou (Nos. QKHJC-ZK[2022]YB009 and QKHJC-ZK[2022]YB014), and the High Level Innovation Talents Project of Guizhou Province (No. ZKHT-GCC[2023]007). The talent introduction start-up funds for scientific research project (GYU-KY-2025).

Declaration of Competing Interest: The authors declare that they have no conflict of interest.

 doi:10.20944/preprints202504.0739.v1

References

1. An, J.; Zhao, X.; Zhang, Y.; Liu, M.; Yuan, J.; Sun, X.; Zhang, Z.; Wang, B.; Li, S.; Li, D. Perspectives of 2D materials for optoelectronic integration. Adv. Funct. Mater. **2022**, *32*, 2110119.
2. Chhowalla, M.; Jena, D.; Zhang, H. Two-dimensional semiconductors for transistors. Nat. Rev. Mater. **2016**, *1*, 1-15.
3. Long, X.; Deng, X.; Hu, F.; Xie, J.; Lv, B.; Liao, Y.; Wang, W. Tunable valley characteristics of WSe_2 and WSe_2/VSe_2 heterostructure. Appl. Surf. Sci. **2023**, *624*, 157111.
4. Dhakal, K.P.; Roy, S.; Jang, H.; Chen, X.; Yun, W.; Kim, H.; Lee, J.; Kim, J. Local strain induced band gap modulation and photoluminescence enhancement of multilayer transition metal dichalcogenides. Chem. Mater. **2017**, *29*, 5124-5133.
5. Dai, T.; Liu, Y.; Fan, X.; Liu, X.; Xie, D.; Li, Y. Synthesis of few-layer 2H-$MoSe_2$ thin films with wafer-level homogeneity for high-performance photodetector. Nanophotonics **2018**, *7*, 1959-1969.
6. Kurpas, M.; Junior, P.; Gmitra, M.; Fabian, J. Spin-orbit coupling in elemental two-dimensional materials. Phys. Rev. B. **2019**, *100*, 125422.
7. Jin, C.; Regan, E.C.; Yan, A.; Utama, M.; Wang, D.; Zhao, S.; Qin, Y.; Yang, S.; Zheng, Z.; Taniguchi, K.; Tongay, S.; Zettl, A.; Wang, F. Observation of moiré excitons in WSe_2/WS_2 heterostructure superlattices. Nature **2019**, *567*, 76–80.
8. Alam, K. Physical insight and performance metrics of monolayer MX_2 heterojunction TFETs. Micro Nano Lett. **2020**, *15*, 81-85.
9. Choukroun, J.; Pala, M.; Fang, S.; Kaxiras, E.; Dollfus, P. High performance tunnel field effect transistors based on in-plane transition metal dichalcogenide heterojunctions. Nanotechnology **2018**, *30*, 025201.
10. Peng, B.; Yu, G.; Liu, X.; Liu, B.; Liang, X.; Bi, L.; Deng, L.; Sum, T.; Loh, K. Ultrafast charge transfer in MoS_2/WSe_2 p–n Heterojunction. 2D Mater. **2016**, *3*, 025020.
11. Policht, V.R.; Russo, M.; Liu, F.; Trovatallo, C.; Maiuri, M.; Bai, Y.; Zhu, X.; Conte, S.; Cerullo, G. Dissecting interlayer hole and electron transfer in transition metal dichalcogenide heterostructures via two-dimensional electronic spectroscopy. Nano Lett. **2021**, *21*, 4738-4743.
12. Conte, S.; Trovatello, C.; Gadermaier, C.; Gerullo, G. Ultrafast photophysics of 2D semiconductors and related heterostructures. Trends Chem. **2020**, *2*, 28-42.
13. Jin, C.; Ma, E.; Karni, O.; Regan, E.C.; Wang, F.; Heinz, T.F. Ultrafast dynamics in van der Waals heterostructures. Nat. Nanotechnol. **2018**, *13*, 994-1003.
14. Varghese, A.; Saha, D.; Thakar, K.; Jindal, V.; Ghosh, S.; Medhekar, N.; Ghosh, S.; Lodha, S. Near-direct bandgap WSe_2/ReS_2 type-II pn heterojunction for enhanced ultrafast photodetection and high-performance photovoltaics. Nano lett. **2020**, *20*, 1707-1717.
15. Ornelas, C.D.; Bowman, A.; Walmsley, T.S.; Wang, T.; Andrews, K.; Zhou, Z.; Xu, Y. Ultrafast photocurrent response and high detectivity in two-dimensional $MoSe_2$-based heterojunctions. ACS Appl. Mater. Interfaces **2020**, *12*, 46476-46482.
16. Ugeda, M.M.; Bradley, A.J.; Shi, S.; Jornada, F.; Zhang, Y.; Qiu, D.Y.; Ruan, W.; Mo, S.; Hussain, Z.; Wang, F.; Louie, S.G.; Crommie, M.F. Giant bandgap renormalization and excitonic effects in a monolayer transition metal dichalcogenide semiconductor. Nat. Mater. **2014**, *13*, 1091-1095.
17. Ding, X.; Zhao, Y.; Xiao, H.; Qiao, L. Engineering Schottky-to-Ohmic contact transition for 2D metal–semiconductor junctions. Appl. Phys. Lett. **2021**, *1*, 18.
18. Y. Wang, M. Chhowalla, Making clean electrical contacts on 2D transition metal dichalcogenides, Nat. Rev. Phys. **2022**, *4*, 101-112.

 doi:10.20944/preprints202504.0739.v1

19. Ross, J.S.; Klement, P.; Jones, A.M.; Ghimire, N.J.; Yan, J.; Mandrus, D.G.; Taniguchi, T.; Watanabe, K.; Kitamura, K.; Yao, W.; Cobden, D.H.; Xu, X. Electrically tunable excitonic light-emitting diodes based on monolayer WSe_2 p–n junctions. Nat. Nanotechnol. **2014**, *9*, 268-272.
20. Baugher, B.W.H.; Churchill, H.O.H.; Yang, Y.; Jarillo-Herrero, P. Optoelectronic devices based on electrically tunable p–n diodes in a monolayer dichalcogenide. Nat. Nanotechnol. **2014**, *9*, 262-267.
21. Liu, Y.; Guo, J.; Zhu, E.; Liao, L.; Lee, S.; Ding, M.; Shakir, I.; Gambin, V.; Huang, Y.; Duan, X. Approaching the Schottky–Mott limit in van der Waals metal–semiconductor junctions. Nature **2018**, *557*, 696-700.
22. Chen, J.; Zhang, Z.; Guo, Y.; Robertson, J. Metal contacts with Moire interfaces on WSe_2 for ambipolar applications. Appl. Phys. Lett. **2022**, *121*, 051602.
23. Lizzit, D.; Khakbaz, P.; Driussi, F.; Pala, M.; Esseni, D. Ohmic behavior in metal contacts to n/p-type transition-metal dichalcogenides: Schottky versus tunneling barrier trade-off. ACS Appl. Nano Mater. **2023**, *6*, 5737-5746.
24. Noori, K.; Xuan, F.; Quek, S. Origin of contact polarity at metal-2D transition metal dichalcogenide interfaces. 2D Mater. Appl. **2022**, *6*, 73.
25. Wang, T.; Jin, H.; Li, J.; Wei, Y. Toward barrier free contact to $MoSe_2/WSe_2$ heterojunctions using two-dimensional metal electrodes. Nanotechnology **2018**, *30*, 015707.
26. Sotthewes, K.; Bremen, R.; Dollekamp, E.; Boulogne, T.; Nowakowski, K.; Kas, D.; Zandvliet, H.J.W.; Bampoulis, P. Universal Fermi-level pinning in transition-metal dichalcogenides. J. Phys. Chem. C. **2019**, *123*, 5411-5420.
27. Li, S.; Chen, J.; He, X.; Zheng, Y.; Yu, C.; Lu, H. Comparative study of the micro-mechanism of charge redistribution at metal-semiconductor and semimetal-semiconductor interfaces: Pt(Ni)-MoS_2 and Bi-MoS_2(WSe_2) as the prototype. Appl. Surf. Sci. **2023**, *623*, 157036.
28. Pande, G.; Sian, J.; Chen, W.; Lee, C.; Sankar, R.; Chang, Y.; Chen, C.; Chang, W.; Chou, F.; Lin, M. Ultralow Schottky barriers in hexagonal boron nitride-encapsulated monolayer WSe_2 tunnel field-effect transistors. ACS Appl. Mater. Interfaces **2020**, *12*, 18667-18673.
29. Farmanbar, M.; Brocks, G. Controlling the Schottky barrier at MoS_2/metal contacts by inserting a BN monolayer. Phys. Rev. B. **2015**, *91*, 161304.
30. Chuang, S.; Battaglia, C.; Azcatl, A.; McDonnel, S.; Kang, J.; Yin, X.; Tosun, M.; Kapadia, R.; Fang, H.; Wallace, R.M.; Javey, A. MoS_2 p-type transistors and diodes enabled by high work function MoOx contacts. Nano lett. **2014**, *14*, 1337-1342.
31. Kaushik, N.; Karmakar, D.; Nipane, A.; Karande, S.; Lodha, S. Interfacial n-doping using an ultrathin TiO_2 layer for contact resistance reduction in MoS_2. ACS Appl. Mater. Interfaces **2016**, *8*, 256-263.
32. Chanana, A.; Mahapatra, S. Prospects of zero Schottky barrier height in a graphene-inserted MoS_2-metal interface. J. Appl. Phys. **2016**, *119*, 014303.
33. Chee, S.; Seo, D.; Kim, H.; Jang, H.; Lee, S.; Moon, S.; Lee, K.; Kim, S.; Choi, H.; Ham, M. Lowering the Schottky barrier height by graphene/Ag electrodes for high-mobility MoS_2 field-effect transistors. Adv. Mater. **2019**, *31*, 1804422.
34. Jang, J.; Kim, Y.; Chee, S.; Kim, H.; Whang, D.; Kim, G.; Yun, S. Clean interface contact using a ZnO interlayer for low-contact-resistance MoS_2 transistors. ACS Appl. Mater. Interfaces **2019**, *12*, 5031-5039.

 doi:10.20944/preprints202504.0739.v1

35. Tran, K.; Moody, G.; Wu, F.; Lu, X.; Choi, J.; Kim, K.; Rai, A.; Sanchez, D. A.; Quan, J.; Singh, A.; Embley, J.; Zepeda, A.; Campbell, M.; Autry, T.; Taniguchi, T.; Watanabe, K.; Lu, N.; Banerjee, S. K.; Silverman, K. L.; Kim, S.; Tutuc, E.; Yang, L.; MacDonald, A.H.; Li, X. Evidence for moiré excitons in van der Waals heterostructures. Nature **2019**, *567*, 71-75.
36. Seyler, K.L.; Rivera, P.; Yu, H.; Wilson, N.P.; Ray, E.L.; Mandrus, D.G.; Yan, J.; Yao, W.; Xu, X. Signatures of moiré-trapped valley excitons in $MoSe_2/WSe_2$ heterobilayers. Nature **2019**, *567*, 66-70.
37. Jauregui, L.A.; Joe, A.Y.; Pistunova, K.; Wild, D.S.; Hign, A.A.; Zhou, Y.; Scuri, G.; Greve, K.; Sushko, A.; Yu, C.; Taniguchi, T.; Watanabe, K.; Needleman, D.J.; Lukin, M.D.; Park, H.; Kim, P. Electrical control of interlayer exciton dynamics in atomically thin heterostructures. Science **2019**, *366*, 870-875.
38. Perdew, J.P.; Burke, K.; Ernzerhof, M. Generalized gradient approximation made simple. Phys. Rev. Lett. **1996**, *77*, 3865.
39. Methfessel, M.; Paxton, A.T. High-precision sampling for Brillouin-zone integration in metals, Phys. Rev. B. **1989**, *40*, 3616.
40. Blöchl, P.E.; Jepsen, O.; Andersen, O.K. Improved tetrahedron method for Brillouin-zone integrations, Phys. Rev. B. **1994**, *49*, 16223.
41. Kang, J.; Liu, W.; Sarkar, D.; Jena, D.; Banerjee, K. Computational study of metal contacts to monolayer transition-metal dichalcogenide semiconductors. Phys. Rev. X. **2014**, *4*, 031005.
42. Kang, J.; Liu, W.; Banerjee, K. High-performance MoS_2 transistors with low-resistance molybdenum contacts. Appl. Phys. Lett. **2014**, *104*, 233502.
43. Morales, J.; Santos, J.; Tirado, J.L. Electrochemical studies of lithium and sodium intercalation in $MoSe_2$. Solid State Ionics **1996**, *83*, 57-64.
44. Al-Hilli, A.A.; Evans, B.L. The preparation and properties of transition metal dichalcogenide single crystals. J. Cryst. Growth **1972**, *15*, 93-101.
45. Kang, J.; Sarkar, D.; Liu, W.; Jena, D.; Banerjee, K. A computational study of metal-contacts to beyond-graphene 2D semiconductor materials. IEEE International Electron Devices Meeting **2012**, 407–410.
46. Wang, Y.; Yang, R.; Quhe, R.; Zhong, H.; Cong, L.; Ye, M.; Ni, Z.; Song, Z.; Yang, J.; Shi, J.; Li, J.; Lu, J. Does p-type ohmic contact exist in WSe_2–metal interfaces? Nanoscale **2016**, *8*, 1179-1191.
47. Pan, Y.; Li, S.; Ye, M.; Quhe, R.; Song, Z.; Wang, Y.; Zheng, J.; Pan, F.; Guo, W.; Yang, J.; Lu, J. Interfacial properties of monolayer $MoSe_2$–metal contacts. J. Phys. Chem. C. **2016**, *120*, 13063-13070.
48. Zheng, J.; Wang, Y.; Wang, L.; Quhe, R.; Ni, Z.; Mei, W.; Gao, Z.; Yu, D.; Shi, J.; Lu, J. Interfacial properties of bilayer and trilayer graphene on metal substrates. Sci. Rep. **2013**, *3*, 2081.
49. Liu, W.; Kang, J.; Sarkar, D.; Khatami, Y.; Jena, D.; Banerjee, K. Role of metal contacts in designing high-performance monolayer n-type WSe_2 field effect transistors. Nano lett. **2013**, *13*, 1983-1990.
50. Wu, Q.; Tagani, M.; Zhang, L.; Wang, J.; Xia, Y.; Zhang, L.; Xie, S.; Tian, Y.; Yin, L.; Zhang, W.; Rudenko, A.N.; Wee, A.T.S.; Wong, P.; Qin, Z. Electronic tuning in WSe_2/Au via van der Waals interface twisting and intercalation. ACS Nano. **2022**, *16*, 6541-6551.
51. Kong, L.; Zhang, X.; Tao, Q.; Zhang, M.; Dang, W.; Li, Z.; Feng, L.; Liao, L.; Duan, X.; Liu, Y. Doping-free complementary WSe_2 circuit via van der Waals metal integration. Nat. Commun. **2020**, *11*, 1866.
52. Wang, Y.; Kim, J.; Wu, R.J.; Martinez, J.; Song, X.; Yang, J.; Zhao, F.; Mkhoyan, A.; Jeong, H.; Chhowalla, M. Van der Waals contacts between three-dimensional metals and two-dimensional semiconductors. Nature **2019**, *568*, 70-74.
53. Wang, J.; Yao, Q.; Huang, C.; Zou, X. High Mobility MoS_2 transistor with low Schottky barrier contact by using atomic thick h-BN as a tunneling layer. Adv. Mater. **2016**, *28*, 8302-8308.

 doi:10.20944/preprints202504.0739.v1

54. Chee, S.; Seo, D.; Kim, H.; Jang, H.; Lee, S.; Moon, S.; Lee, K.; Kim, S.; Choi, H.; Ham, M. Lowering the Schottky barrier height by graphene/Ag electrodes for high-mobility MoS_2 field-effect transistors. Adv. Mater. **2019**, *31*, 1804422.
55. Park, W.; Kim, Y.; Lee, S.; Jung, U.; Yang, J.; Cho, C.; Kim, Y.; Lim, S.; Hwang, I.; Lee, H.; lee, B. Contact resistance reduction using Fermi level de-pinning layer for MoS_2 FETs. 2014 IEEE International Electron Devices Meeting, **2014**, 5.1.1-5.1. 4.
56. Jiang, J.; Xu, L.; Du, L.; Li, L.; Zhang, G.; Qiu, C.; Peng, L. Yttrium-doping-induced metallization of molybdenum disulfide for ohmic contacts in two-dimensional transistors. Nat. Electron. **2024**, *7*, 545-556.
57. Cowley, A.M.; Sze, S.M. Surface states and barrier height of metal-semiconductor systems. J. Appl. Phys. **1965**, *36*, 3212-3220.